Analytical Letters

ISSN: 0003-2719 (Print) 1532-236X (Online) Journal homepage: https://www.tandfonline.com/loi/lanl20

Electrochemical Determination of Bisphenol A in Saliva by a Novel Three-Dimensional (3D) Printed Gold-Reduced Graphene Oxide (rGO) Composite Paste Electrode

Livia Alexandra Gugoasa, Raluca-Ioana Stefan-van Staden, Jacobus Frederick van Staden, Maria Coroș & Stela Pruneanu

To cite this article: Livia Alexandra Gugoasa, Raluca-Ioana Stefan-van Staden, Jacobus Frederick van Staden, Maria Coro# & Stela Pruneanu (2019) Electrochemical Determination of Bisphenol A in Saliva by a Novel Three-Dimensional (3D) Printed Gold-Reduced Graphene Oxide (rGO) Composite Paste Electrode, Analytical Letters, 52:16, 2583-2606, DOI: 10.1080/00032719.2019.1620262

To link to this article: https://doi.org/10.1080/00032719.2019.1620262

ANALYTICAL LETTERS
2019, VOL. 52, NO. 16, 2583–2606
https://doi.org/10.1080/00032719.2019.1620262

Taylor & Francis
Taylor & Francis Group

SENSORS

Electrochemical Determination of Bisphenol A in Saliva by a Novel Three-Dimensional (3D) Printed Gold-Reduced Graphene Oxide (rGO) Composite Paste Electrode

Livia Alexandra Gugoasa[a], Raluca-Ioana Stefan-van Staden[a], Jacobus Frederick van Staden[a], Maria Coroș[b], and Stela Pruneanu[b]

[a]Laboratory of Electrochemistry and PATLAB, National Institute of Research for Electrochemistry and Condensed Matter, Bucharest-6, Romania; [b]National Institute for Research and Development of Isotopic and Molecular Technologies, Cluj-Napoca, Romania

ABSTRACT

A novel synthesized gold (Au)-reduced graphene oxide composite (rGO) was used for the fabrication of an electroactive paste inserted in a three-dimensional (3D)-printed platform for the determination of bisphenol A (BPA). The proposed method exhibits good response towards oxidation of BPA in the linear concentration range from 1.00×10^{-7} mol L^{-1} to 1.00×10^{-2} mol L^{-1}. The Au-rGO based 3D-printed platform determined BPA with a detection limit of 3.52×10^{-9} mol L^{-1}, in comparison with rGO based 3D-printed platform, where the limit of detection was 3.05×10^{-6} mol L^{-1}. Gold modification of rGO improves the sensitivity and electrochemical behavior of the material for BPA oxidation. The method was validated using five saliva samples collected from children.

ARTICLE HISTORY
Received 18 March 2019
Accepted 14 May 2019

KEYWORDS
Bisphenol A (BPA); cyclic voltammetry (CV); differential pulse voltammetry (DPV); reduced graphene oxide (rGO); three-dimensional (3D) printing

Introduction

Changes that occur in a pubertal period are due to excessive weight gain and exposure to toxic environmental substances. Many substances used in plastic fabrication have been identified as potential endocrine disrupting compounds, having a great impact on the normal development of the reproductive system and on average age of reaching puberty (Berger et al. 2018). Once one of the most generally plastic materials employed worldwide is bisphenol A (BPA), today this substance is forbidden for use as a precursor in the fabrication of plastics, especially those used for toys, baby feeding bottles, and pacifiers (Vandenberg et al. 2010).

Children are the most vulnerable to this toxic material when consumed, much more than adults, due to the fact that BPA migrates from plastic recipients into milk, water or food (Morgan et al. 2011). BPA affects the hormonal balance, which is very important in the growth and development period of a baby or a child (Goldman et al. 2004; DiVall 2013). The amounts of BPA found in urine and blood are responsible for early appearance of second sexual characteristics in boys and girls and also for reaching puberty at early age (Watkins et al. 2017).

CONTACT Livia Alexandra Gugoasa livia.gugoasa@yahoo.com Laboratory of Electrochemistry and PATLAB, National Institute of Research for Electrochemistry and Condensed Matter, 202 Splaiul Independentei Str, Bucharest-6 060021, Romania.
Color versions of one or more of the figures in the article can be found online at www.tandfonline.com/lanl.

Leonardi et al. in their recent review (Leonardi et al. 2017) concluded that BPA plays an important role only in girls that present early onset of puberty or premature thelarche. In many of the studies, they found only hypothesizes of the potential interference with metabolism as an endocrine disruptor (Leonardi et al. 2017). Because of these limitations in the investigation of BPA and its correlation with precocious puberty, our present study presents a fast and easy method for the determination of BPA from biological samples, such as saliva. Our study will allow researchers to evaluate more samples faster, so the molecular mechanism that underlies the activity of BPA as puberty disruptor may be evaluated and elucidated.

From an analytical point of view, electrochemical methods are a good alternative due to their response, simple and easy procedure, high sensitivity and selectivity. For the determination of BPA, since it is an electrochemically active molecule, electrochemical sensors (Stefan-van Staden et al. 2014; Pogacean et al. 2016) have been previously proposed. Classical carbon paste electrodes (CPEs) (Adams, 1958) formed from graphite-based powders mixed with different types of oils for the detection of bisphenol A (Huang, 2005; Li et al. 2016; Ianesko et al. 2018) are presented in Table 1. Also, modified glassy carbon electrodes have been reported in large numbers for determination of bisphenol A from water samples or plastic products (Table 1). To the best of our knowledge, there are few electrochemical methods for determination of BPA from biological samples.

Three-dimensional (3D) printed sensors represent, nowadays, a very good alternative to classical sensors, which can overcome the limitations brought by traditional manufacturing methods such as expensive instrumentation, qualified personnel, and difficult and time-consuming fabrication processes (Xu et al. 2017). Three dimensional (3D)-printing technologies are improving every day and provide many applications such as force sensors (Kesner and Howe, 2011); strain sensors (Frutiger et al. 2015); pressure sensors (Laszczak et al. 2015); displacement sensors (Jerance, Bednar, and Stojanovic 2013); optical sensors (Igrec et al. 2016); electromagnetic sensors (Sanz-Izquierdo and Parker 2014); biosensors (Mandoon, Blum, and Marquette 2016; Lind et al. 2017); chemosensors (Kit-Anan et al. 2012; Kadimisetty et al. 2016); and gas detection sensors (Staymates et al. 2016).

Biological and chemical detection 3D printed sensors are of great interest for the medical field. A 3D-printed electrochemiluminescent protein immunoarray was developed for detection of three cancer biomarkers from biological animal serum samples within 35 min with very low detection limits (0.3–0.5 pg/mL) (Kadimisetty et al. 2016). The future for these 3D printed sensors is promising and is more appropriate for small devices and devices used in implantable therapeutics (Xu, Wang, and Hu 2017).

In the last three decades, graphene became an intensively studied electrode material due to its increased conductivity, high catalytic response, and good biocompatibility (Bharath et al. 2015). Among the techniques developed so far to produce graphene (Bhuyan et al. 2016), the chemical reduction of graphene oxide (GO) is considered the most attractive for many applications because its surface is full of oxygen containing reactive groups which make it a suitable platform for functionalization (Parnianchi et al. 2018). Reduced graphene oxide (rGO), due to its stable structure of single layer of six-membered ring of carbon atoms, possesses special features such as high surface area,

Table 1. Comparison of the electrochemical parameters obtained using modified carbon paste electrodes and modified solid glassy carbon electrodes for the determination of BPA.

Electrode[a]	Method	Detection limit (mol L^{-1})	Sample	References
Modified glassy carbon electrodes (GCEs)				
N-GS-CS/GCE	Cyclic voltammetry Chronoamperometry	5.00×10^{-9}	River water samples	Fan et al. (2012)
MWCNT-AuNPs/GCE	Cyclic voltammetry	4.00×10^{-9}	Water samples	Messaoud et al. (2017)
rGO-Fc-NH_2-AuNPs/GCE	Cyclic voltammetry Differential pulse voltammetry	2.00×10^{-9}	Milk samples	(Huang et al., 2015)
Cu_2O-rGO/GCE	Cyclic voltammetry Chronoamperometry	5.30×10^{-8}	Water samples	Shi et al. (2017)
Gr-AgCu/Au electrode Gr-AuCu/Au electrode	Linear sweep voltammetry	1.31×10^{-6} 1.91×10^{-6}	–	Pogacean et al. (2016)
MB-ssDNAaptamer/AuPET	Linear sweep voltammetry	1.75×10^{-12}	Plastic products	Yu et al. (2019)
MnP/PANI-PMMA-TiO_2/GCE	Cyclic voltammetry Square wave voltammetry	1.70×10^{-10}	–	Sidwaba et al. (2019)
SPE-rGO-CNPs	Differential pulse voltammetry	1.00×10^{-9}	Water samples	Canevari, Rossi, and Alexiou (2019)
Modified carbon paste electrodes (CPEs)				
CTAB/CPE	Cyclic voltammetry	7.50×10^{-9}	Waste plastic products	(Huang, 2005)
CoPC/CPE	Cyclic voltammetry; Square wave voltammetry; Differential pulse voltammetry	0.10×10^{-8}	Plastic products	Yin, Zhou, and Ai (2009)
Thionine-tyrosinase/CPE	Cyclic voltammetry	1.50×10^{-7}	–	Portaccio et al. (2010)
β-CD/IL-CPE	Differential pulse voltammetry	8.30×10^{-8}	Water samples and plastic products	Yu et al. (2013)
MMIPs NPs/CTAB/CPE	Cyclic voltammetry	1.00×10^{-7}	Water samples and plastic products	Zhu, Cao, and Cao (2014)
Ordered mesoporous carbon/IL-CPE	Lienar sweep voltammetry	5.00×10^{-8}	Plastic products	Li et al. (2016)
nAg-PVP/CPE	Cyclic voltammetry; Square wave voltammetry	2.50×10^{-8}	Water samples	Ianesko et al. (2018)
Au-rGO paste based 3D-printed platform	Differential pulse voltammetry	3.52×10^{-9}	Saliva samples from children	This work

aMWCNT: multiwalled carbon nanotubes; -AuNPs: gold nanoparticles; N-GS: nitrogen-doped graphene sheets; CS: chitosan; Cu_2O-rGO: cuprous oxide-reduced graphene oxide; Fc-NH_2: (4-ferrocenylethyne) phenylamine; PMMA: polymethyl methacrylate; PANI: polyaniline: MnP: manganese peroxidase; CNPs: carbon nanoparticles; SPE: screen printed electrode; MB: methylene blue; ssDNAaptamer: single stranded DNA aptamer; AuPET: gold polyethylene terephthalate electrode; m β-CD: β-cyclodextrin; IL: ionic liquid; CPE: carbon paste electrode; MMIPs NPs: magnetic molecularly imprinted polymers nanoparticles; CTAB: cetyltrimethyl ammonium bromide; n-Ag: silver nanoparticles; PVP: polyvinylpyrrolidone; CoPC: cobalt phtalocyanine;.

excellent electrical and thermal conductivity, and exceptional mechanical, electronic, and optical properties.

Graphene–nanoparticle composites have shown great adaptability in the manufacture of electrochemical sensors and biosensors with excellent analytical properties demonstrated in the detection of organic molecules (Xu, Wang, and Hu 2017). Two bimetallic-graphene composites were used previously as sensor materials for the quantitative detection of BPA reaching micromolar detection limits (Pogacean et al. 2016). Many rGO sensors often modified with noble metal particles, such as Ag (Kalambate et al. 2016), Au (Wang, Cokeliler, and Gunasekaran 2015), Pt (Wan et al. 2016), and Pd (Yang et al. 2014), have been used for BPA detection. For most work, these sensors were not employed for analysis of biological samples. For biological samples, some other analytical methods have been employed (Table 2).

In this publication, a electrochemical 3D printed platform used a paste based electrode for the working electrode, which covers the necessary concentration range of BPA from 1.0×10^{-7} to 1.0×10^{-2} mol L^{-1} for the analysis of biological samples collected from pre-pubertal children. Because the concentration of BPA in children̓s body during puberty time is high, a very low limit of detection was not a goal for this publication. Also, being a paste electrode, its surface is very rapidly renewed, easily be used by personnel without medical qualification, and inexpensive comparing to chromatographic methods. The amount of saliva samples needed is very small (less than 1 mL) and the measurement of the samples is done within minutes. With the method proposed in this publication, only one sample can be analyzed at a time, while ELISA method needs many more samples at once to use the measurement kit.

Saliva samples represent noninvasive biological samples and are safer and easier collected from infants or children. Also, it is easier to obtain consent from parents to collect saliva from their offspring than to collect blood or urine samples. BPA was investigated from saliva samples in previous studies (Yang et al. 2011; Stefan-van Staden et al. 2014).

In this study, gold nanoparticles-reduced graphene oxide composite (Au-rGO) was proposed as the material for the working electrode. The obtained modified Au-rGO paste was inserted in a 3D printed platform used for the rapid determination of BPA from saliva samples from children.

Experimental

Materials and reagents

Reduced-graphene oxide nanopowder, bisphenol A (BPA), potassium ferricyanide, dimethylsulfoxide (DMSO), monosodium phosphate, disodium phosphate, potassium chloride, sodium chloride, potassium nitrate and paraffin oil (d_4^{20}, 0,86 g cm^{-1}) were purchased from Sigma Aldrich (Milwaukee, USA). Chloroauric acid ($HAuCl_4$) and sodium ascorbate were purchased from Alfa–Aesar (Germany). Distilled water obtained from a Millipore Direct-Q3 system (Molsheim, France) was used for the preparation of all solutions.

Monosodium phosphate and disodium phosphate were used to prepare buffer solutions of different pH values equal to 6.0; 6.5; 7.0; 7.5; and 8.0. Potassium ferricyanide

Table 2. Analytical methods employed for the determination of BPA in biological samples.

Method[1]	Limit of detection	Biological sample	References
HPLC-ED	0.05 ng mL^{-1}	Serum	Inoue et al. (2000)
	0.20 ng mL^{-1}	Urine	Ouchi and Watanabe (2002)
HPLC-FL	0.05 ng mL^{-1}	Serum/plasma	Watanabe et al. (2001)
	0.11 ng mL^{-1}	Breast milk	Sun et al. (2004)
LC-EI-MS	49 pg mL^{-1}	Saliva	Yang et al. (2011)
Amperometric sensors	0.056 nmol L^{-1}	Serum	Zhu et al. (2015)
Amperometric/ stochastic sensors	9.92 pmol L^{-1} 1.00 fmol L^{-1}	Saliva	Stefan-van Staden et al. (2014)
GC-MS	15.00 pg mL^{-1}	Serum	Sajiki, Takahashi, and Yonekubo (1999)
	0.10 ng mL^{-1}	Urine	Kuklenyik et al. (2003) Tsukioka et al. (2003)
ELISA	0.03 ng mL^{-1}	Urine	Lei et al. (2013)
	0.20 ng mL^{-1}	Maternal serum	Yamada et al. (2002)

[1]LC – liquid chromatography; HPLC – high performance liquid chromatography; EI – electronspray ionization; MS – mass sprectrometry; GC-gas chromatography; ELISA – enzyme linked immunosorbent assay; FL – fluorescence; ED – electrochemical detection.

stock solution (10^{-1} mol L^{-1}) was prepared in distilled water. BPA stock solution (10^{-1} mol L^{-1}) was prepared in dimethylsulfoxide. Serial dilution was used for the preparation of different concentration for BPA solutions (10^{-12} mol L^{-1} to 10^{-2} mol L^{-1}) prepared in phosphate buffer solution at pH 7.4. When not in use, all solutions were stored at room temperature in a drawer.

Preparation of Au-rGO composite

For the preparation of the Au-rGO composite, 300 mg graphene oxide synthesized by a modified Hummers method (Pruneanu et al. 2015) were sonicated in 80 mL H_2O for 25 min.Next, 129 μL of 1% chloroauric acid were added. The resulting mixture was stirred for 2 h at room temperature and a solution of sodium ascorbate (800 mg in 5 mL H_2O) was added in order to simultaneously reduce both the gold precursor and graphene oxide and stirred for another 30 min at room temperature. The mixture was heated to 90–100 °C and maintained at this temperature for 3 h. The resulting homogeneous black suspension was filtered, washed with water several times, and dried by lyophilization.

Design of 3D printed platform based on Au-rGO composite

3D-printed platform

The Stratasys objet 24 printer uses the polyjet technology to build 3D models layer-by-layer. The material used is vero white plus – a rigid white opaque polymer. The support material fullcure 705 is an acrylic, easily washable, nontoxic gel-like photopolymer. The printer accuracy was 0.1 mm. The operating temperature was 18–25 °C, and the relative humidity 30–70%.

The time needed for printing the model shown in Figure 1 was 2 h and 18 min. The model was printed in a glossy polymer and placed vertically on the printing table to diminish the amount of support material used. The surface diameter of the working electrode was 300 μm.

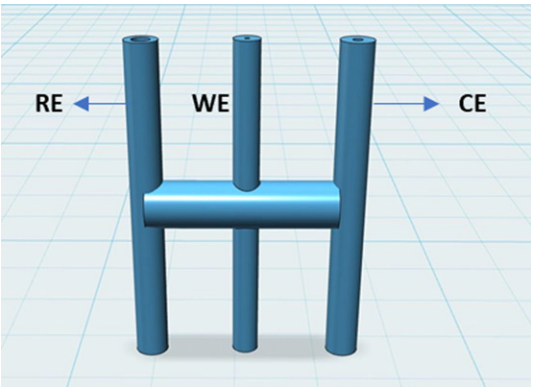

Figure 1. Schematic design of 3D printed platform where is the RE Ag/AgCl reference electrode; WE is the working electrode; and CE is the Pt wire counter electrode.

Preparation of graphene pastes

Graphene based powders (rGO and Au-rGO) were mixed with paraffin oil until homogenous pastes were obtained. The pastes were placed in the middle cylinder of the 3D printed platform (Figure 1). A silver wire was used for the electrical contact (0.3 mm in diameter). A Ag/AgCl sensor and Pt wire served as reference and auxiliary electrodes in the cell. Before each measurement, the sensors were cleaned with deionized water. When not in use, they were stored in a dry place at room temperature.

Apparatus and methods

All electrochemical measurements were performed with a potentionstat/galvanostat Autolab PGSTAT 100 (Methrom, Utrecht, The Netherlands) connected to a personal computer. To record the measurements, GPES and NOVA 2.1 software were used. All measurements were carried out at 25 °C.

For electrochemical impedance (EIS) measurements, an Ivium Compactstat was used. IviumSoft and Ivifit software were used to interpret and fit the results.

For the 3D printed platform, a Stratasys objet 24 3D printer, connected to a personal computer, was employed using Objetstudio^{TM} as the printing software. 123 design was the software used to design the support for the electrochemical cell.

For preliminary electrochemical characterization of the 3D printed electrochemical platforms, cyclic voltammetry (CV) and differential pulse voltammetry (DPV) were employed. Differential pulse voltammetry parameters were optimized and presented in Table 3.

The morphology of the Au-rGO composite was investigated by transmission electron microscopy (TEM), scanning electron microscopy (SEM) and scanning transmission electron microscopy (STEM) with energy dispersive X-ray (EDX) spectroscopy for the elemental mapping of atom (C, Au, O) distribution (SU-8230 STEM system, Hitachi, Japan).

X-ray powder diffraction (XRD) patterns were recorded with Diffrac Plus XRD Commander with a Bruker D8 advance diffractometer (40 kV, 0.5 mA) equipped with a Lynexe detector employing a scan speed of 0.02° s^{-1} and using $CuK_{\alpha 1}$ radiation at a

Table 3. Working parameters used in differential pulse voltammetry for the determination of BPA.

Differential pulse voltammetry parameter	Value
Potential range (V)	0.2–1.0
Step potential (V)	0.05
Modulation amplitude (V)	0.025
Scan rate (V/s)	0.1

wavelength of 1.5406 Å. A Ge (111) monochromator in the incident beam was used in order to increase the resolution and to remove the $K_{\alpha 2}$ radiation. Before plotting the experimental results, the spectrum background was corrected. The background correction of the patterns was performed in the WinPLOTR software.

A Christ Alpha 1-4 LSC freeze dryer was used for sample lyophilization.

Saliva samples

Five saliva samples were collected from children patients in the same morning before 9 a.m., almost 12 h since the last meal, drink and mouth wash. Saliva samples were collected following a mouth rinse with water. Approximately 2 mL of saliva was collected from each child and after centrifugation, the samples were stored in a freezer (–80 °C) in 1 mL aliquots. The ethics committee approval was number 158/2018, awarded by the University of Medicine and Pharmacy "Carol Davila" in Bucharest. Informed consent was obtained from all parents or legal tutors of the patients.

The samples were analyzed using the proposed sensors, without any sample pretreatment and the differential pulse voltammetry measurements were performed in the same day using the proposed 3D printed platform.

The percentile of body mass index (BMI) was categorized as follows: obese children >95th percentile; overweight children: 85th–95th percentile and normal weight children: <85th percentile (Centers for Disease Control and Prevention 2019).

Results and discussion

Morphological and structural characterization of Au-rGO composite

Figure 2 shows the typical scanning electron and transmission electron micrographic (SEM, TEM) images of the composite material, Au-rGO. TEM images reveal the wrinkled morphology of the graphene sheets with attached gold nanoparticles (the dark spots shown in Figure 2a). The gold nanoparticles are barely visible in the SEM images because they are trapped between the graphene sheets.The edges of the graphene sheets are represented by the bright lines (Figure 2b).

In order to determine the elemental distribution within the Au-rGO composite, STEM-EDX mapping was employed (Figure 3). The spectrum in Figure 3b clearly ilustrates the presence of carbon and gold with a small percentage of oxygen (3.3 wt%) which originates from the graphene oxide sheet.

The choice of the reducing agent is very important since the most popular, hydrazine and hydrazine derivatives are toxic and may contaminate the final product. Alternatively, the employment of sodium ascorbate leads to a green and rapid reduction method with nontoxic solvents. In this case, this reducing agent was shown to be highly

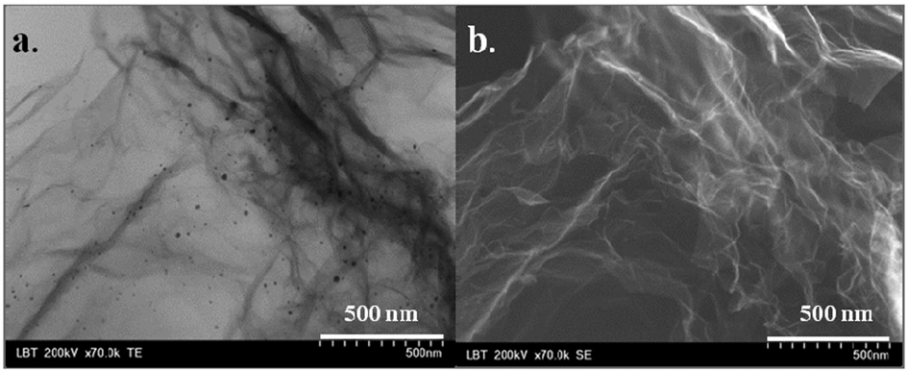

Figure 2. (a) Transmission electron microscopy and (b) scanning electron microscopy images of the Au-rGO sample. Scale bar 500 nm; magnification 70,000×; accelerating voltage 200 kV.

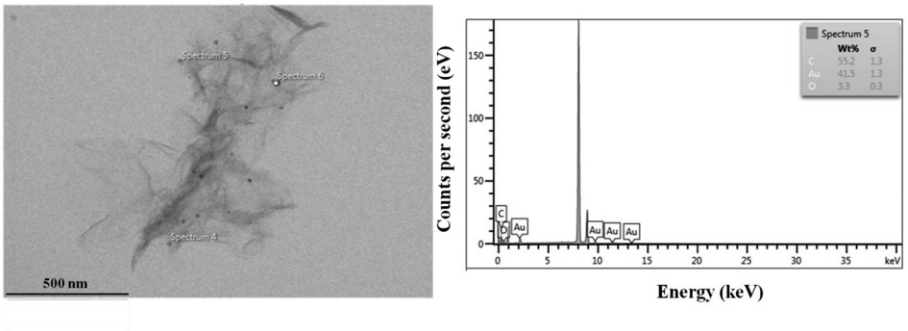

Figure 3. Representative transmission electron microscopy image of (a) Au-rGO. Scale bar 500 nm; magnification 70,000×; accelerating voltage 200 kV. (b) Corresponding energy dispersive X-ray spectroscopy analysis: C 55.2 wt%; Au 41.5 wt%; O 3.3 wt%.

effective as demonstrated by the XRD pattern of the sample. Thus, we observe the almost complete disappearance of the diffraction line from 2θ equal to 11.91°, corresponding to graphene oxide (GO, Figure 4), and the presence of the characteristic band of reduced graphene oxide (rGO) at $2\theta = 22.19°$ (Figure 4). Additionally, peaks related to the (111), (200), (220), (311) and (222) reflections of gold are observed, which demonstrate the successful formation of the Au-graphene composite.

XRD provides three types of structural information: the number of graphene layers (n), the interlayer distance (d) and the mean crystallite size (D). The mean crystallite sizes of graphene (D equal to 0.98 nm) and of gold nanoparticles (D equal to 24.7 nm) attached to graphene were determined using the Scherrer equation (Srinivas et al. 2010). The interlayer distance was found using Bragg's equation (Jun 2015), while the average number of layers was determined from the relationship $n=D/d$.

The structural parameters obtained from the diffraction data are presented in Table 4. The starting material, graphene oxide, had seven layers (D equal to 5.197 nm) and after the nanoparticle deposition and simultaneous reduction, the final material consisted of bilayer graphene with a 0.401 nm interlayer distance.

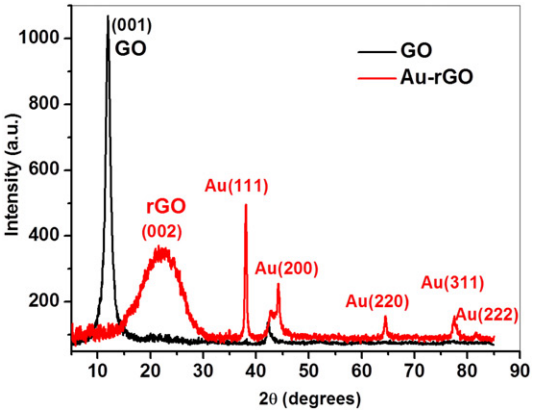

Figure 4. X-ray diffraction pattern of graphene oxide and the Au-rGO composite, showing distinct diffraction peaks for graphene and gold. JCPDS file number 04-0784; a scan speed of 0.02° s^{-1} was employed using monochromatic Cu $K_{\alpha 1}$ radiation.

Table 4. Structural parameters of GO and Au-rGO samples from XRD pattern: graphene crystallite size (*D*), interlayer distance (*d*), and average number of layers (*n*).

Sample	2θ (degrees)	Graphene crystallite size (*D*) (nm)	Interlayer distance (*d*) (nm)	Average number of layers (*n*)
GO	11.91	5.197	0.7404	7
Au-rGO	22.2	0.98	0.401	2

Electrochemical characterization of graphene based 3D-printed platform

The preliminary electrochemical characteristics of the Au-rGO and rGO based 3D-printed platforms were characterized by cyclic voltammetry and electrochemical impedance spectroscopy.

Cyclic voltammograms were recorded in $K_3[Fe(CN)_6]$ (0.1 mol L^{-1} in 0.1 mol L^{-1} KNO_3 supporting electrolyte) with rGO and Au-rGO based 3D-printed platform at a scan rate of 100 mV/s. The results are shown in Figure 5a. In the case of Au-rGO based 3D printed platform, the anodic and cathodic peak currents are well defined and the peak potential separation is 60 mV, characteristic of a reversible redox systems. In contrast, for the rGO based 3D printed platform, the peak currents are considerably lower by more than three times and the peak potential separation is 300 mV, characteristic of quasi-reversible redox systems. The differences between the two electrodes were even further demonstrated by the use of electrochemical impedance spectroscopy.

The impedance spectra were recorded between 0.1 and 10^6 Hz and were interpreted based on an equivalent electrical circuit (Figure 5b inset). This circuit contains the solution resistance (R_s), the Warburg impedance (Z_W) in series with the charge–transfer resistance (R_{ct}), and a constant phase element (CPE) that replaces the double layer capacitance (Bard and Faulkner 1980). The constant phase element arises due to the roughness of the electrode surface, porosity and dynamic disorder associated with diffusion (Ganesh, Pitchumani, and Lakshminarayanan 2006).

The R_{ct} values for the two electrodes were determined by fitting the experimental data with the proposed equivalent electrical circuit. In the case of rGO based 3D printed platform, its value can be also obtained from the high-frequency semicircle. Figure 5b

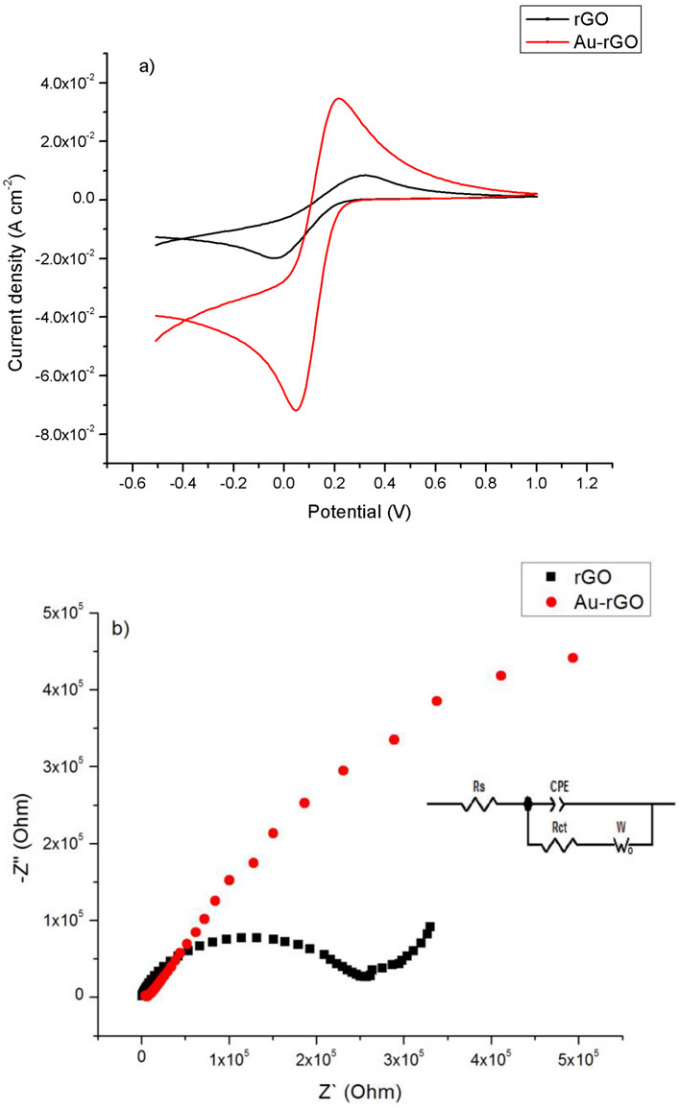

Figure 5. Cyclic voltammograms in 0.1 mol L^{-1} $K_3[Fe(CN)_6]^{3-/4-}$ solution in 0.1 mol L^{-1} KNO_3. Conditions: potential range: –0.5 to 1.0 V; step potential: 0.01 V. (b) Electrochemical impedance spectra of 3D-printed platforms containing rGO paste (black) in comparison with Au-rGO paste (red) in 5.0 mmol L^{-1} $K_3[Fe(CN)_6]^{3-/4-}$ solution in 0.1 mol L^{-1} KNO_3. The frequency range was between 0.1 and 10^6 Hz. Inset: equivalent circuit diagram of the electrochemical interface used to fit the impedance spectra where Rs is solution resistance; Zw is the Warburg diffusion resistance; Rct is the electron–transfer resistance, and CPE is the constant phase element.

shows that for rGO based 3D printed platform, the R_{ct} value is very large (2.9×10^5 Ω), indicating a slow transfer of electrons between the $[Fe(CN)_6]^{3-}$ ions and the electrode surface. In contrast, the Au-rGO based 3D printed platform has a considerably lower value for R_{ct}, equal to 300 Ω, which highly favors the electron transfer during the oxidation of $[Fe(CN)_6]^{3-}$ to $[Fe(CN)_6]^{4-}$.

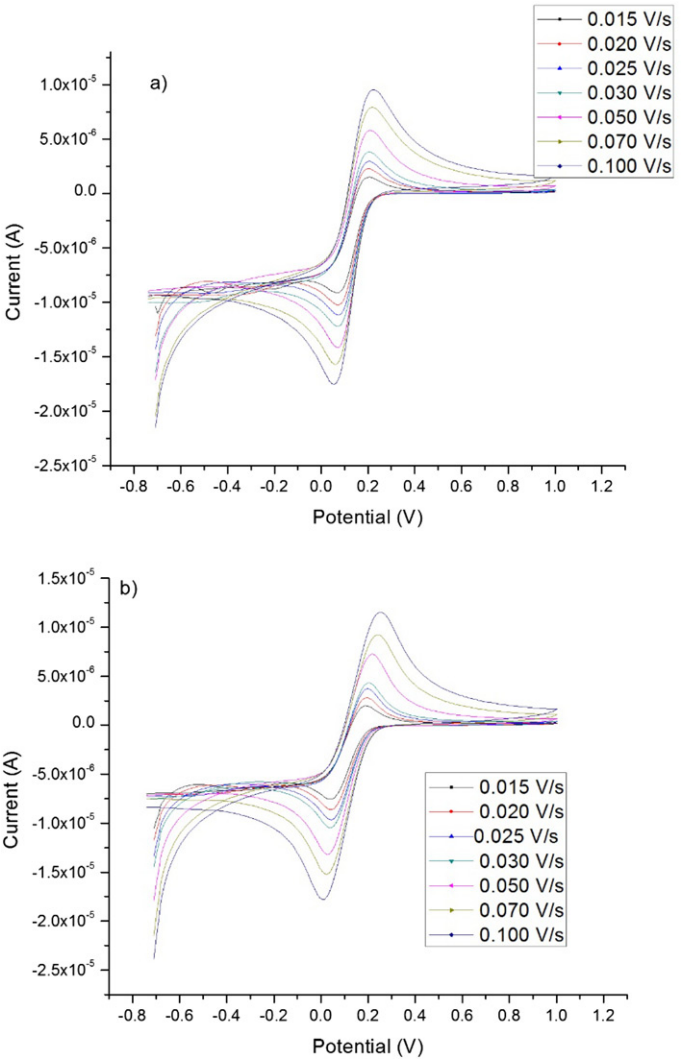

Figure 6. Cyclic voltammograms recorded with various scanning rates in 0.1 mol L^{-1} $K_3[Fe(CN)_6]$ using the 3D printed platform based on (a) rGO and (b) Au-rGO. Conditions: potential range from −0.7 to 1.0 V; step potential of 0.01 V.

Based on the electron–transfer resistance calculated for each electrode from the corresponding impedance spectra, the apparent electron transfer rate constant (k_{app}) was determined by (Nkosi et al. 2010):

$$K_{app} = \frac{RT}{n^2F^2AR_{ct}C} \quad (1)$$

where n is the number of electrons transferred during the redox reaction; F is the Faraday constant (96485 C/mol); R is the ideal gas constant (8.314 J/(mol K)); T is the temperature (298 K); A is the active area of the electrode (cm^2); R_{ct} is the charge–transfer resistance obtained from the fitted Nyquist plots (Ω); and C is the concentration of the redox species (mol/cm^3).

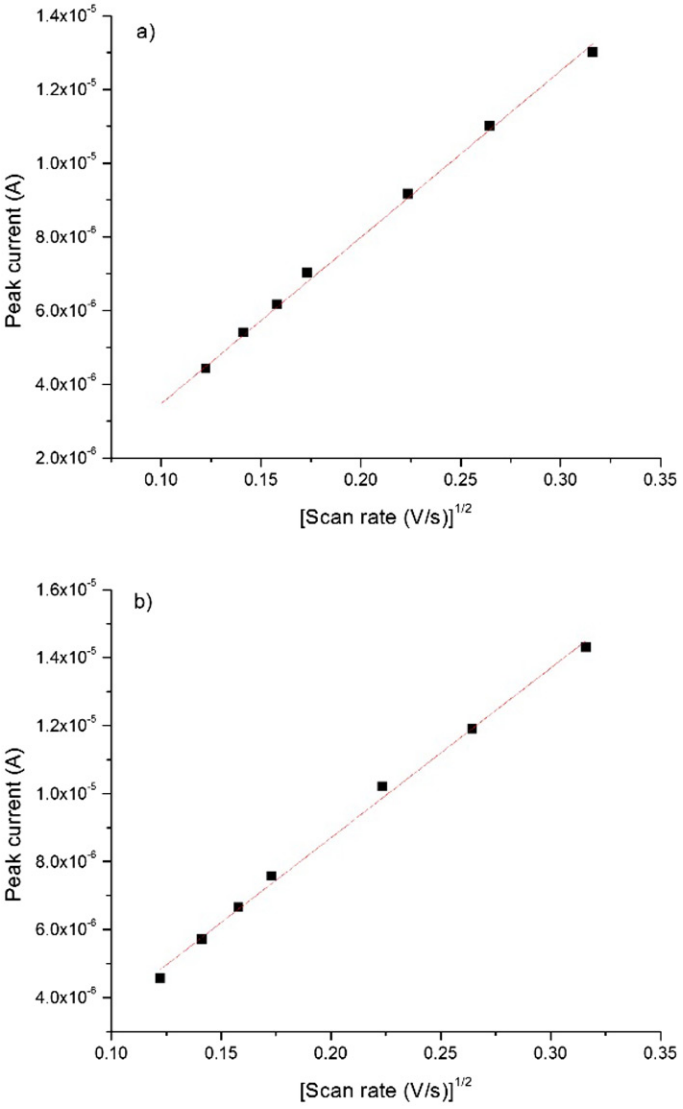

Figure 7. Linear regression of the anodic peak current for the 3D printed platform based on (a) rGO (r equal to 0.9980) where Ipa=$-8.29 \times 10^{-7}+4.42 \times 10^{-5} \times v^{1/2}$ and (b) Au-rGO (r equal to 0.9982) where Ipa=$-1.29 \times 10^{-6}+4.99 \times 10^{-5} \times v^{1/2}$.

In the case of rGO based 3D-printed platform, K_{app} was determined to be 2.77×10^{-4} cm/s, which is three orders of magnitude smaller than the value corresponding to the rGO-Au electrode (2.37×10^{-1} cm/s). This difference may be attributed to gold nanoparticles attached to graphene surface which enhances the transfer of electrons.

Effect of scan rate – Surface area study

Cyclic voltammetry was employed to study the surface area of the rGO and Au-rGO pastes using a 0.1 mol L^{-1} $[Fe(CN)_6]^{3-/4-}$ redox couple. The influence of the scan rate

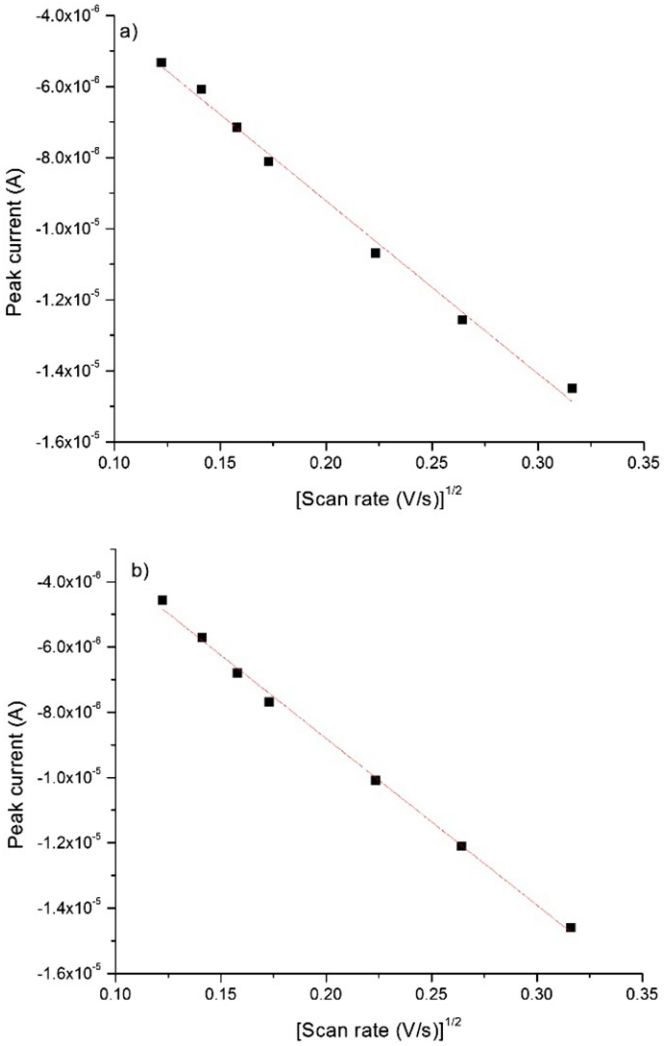

Figure 8. Linear regression of the cathodic peak current for the 3D printed platform based on (a) rGO ($r = 0.9971$) and (b) Au-rGO ($r = 9988$).

on the redox process of 0.1 mol L^{-1} $K_3[Fe(CN)_6]$ using these graphene-based 3D-printed platforms are shown in Figure 6.

Using the Randles–Sevcik equation, which describes the process of a reversible redox couple, the peak current is direct proportional with the square root of scan rate ($\upsilon^{1/2}$) (Zanello, 2003):

$$\mathrm{Ip} = \pm(2.69 \times 10^5)\, n^{3/2} \mathrm{A} \mathrm{C}_0 \mathrm{D}_\mathrm{R}{}^{1/2} \upsilon^{1/2} \tag{2}$$

where Ip is the anodic peak current (A), n is the number of electrons involved in the redox reaction (in this case, $n = 1$), A is the active surface area of the electrode (cm^2), C_0 is the concentration of $K_3[Fe(CN)_6]$ (mol cm^{-3}), and υ is the scan rate (V/s).

The diffusion coefficient D_R is equal to 6.20×10^{-6} cm^2 s^{-1} at a temperature of 25 °C (298.15 K). For scan rates from 15 to 100 mV/s, both anodic and cathodic peaks (Ip_a

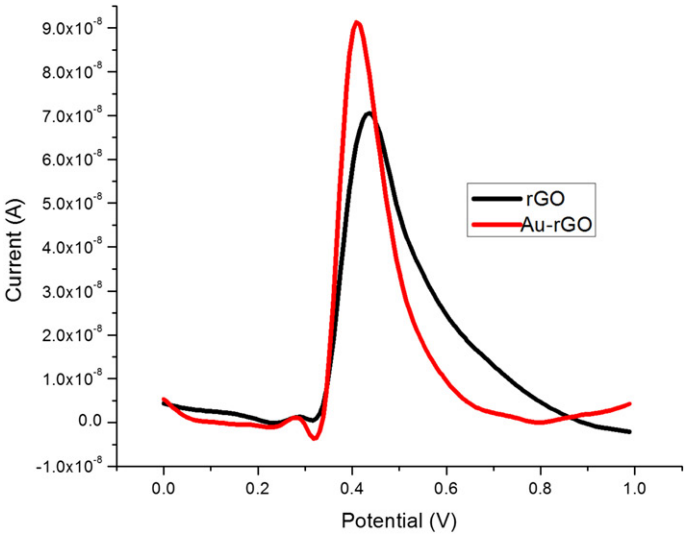

Figure 9. Differential pulse voltammograms recorded using 3D-printed platforms based on rGO and Au-rGO in a solution of 1×10^{-3} mol L^{-1} BPA in pH 7.4 phosphate buffer and 0.1 mol L^{-1} KCl. Working conditions: step potential of 0.05 V; modulation amplitude of 0.025 V; and 0.100 V/s scan rate.

and Ip_c) obtained with the graphene-based 3D printed platform depend linearly on the square root of the scan rate (Figures 7 and 8), indicating a redox process controlled by diffusion. Thus, from Eq. (2), the surface areas (A) of the proposed paste based 3D printed platforms were determined to be 0.066 mm^2 for rGO based 3D printed platform and 0.074 mm^2 for Au-rGO based 3D printed platform.

Repeatability

The repeatability of Au-rGO and rGO based 3D-printed platforms was investigated by five replicate cyclic voltammograms recorded in 0.1 mol L^{-1} $K_3[Fe(CN)_6]$. A set of five 3D printed platforms using each paste were newly built at the beginning of each day. The relative standard deviation calculated for the peak currents was 5.60% for the rGO based 3D-printed platform and 6.50% for the Au-rGO based 3D-printed platform. These relative standard deviations demonstrate the good repeatability of the peak current responses obtained with the proposed 3D printed platforms in a solution of 0.1 mol L^{-1} $K_3[Fe(CN)_6]$.

Regarding the 3D-printed platforms described above, the Au-rGO-based platform showed a higher analytical signal when introduced into a solution containing 10^{-3} mol L^{-1} BPA, pH 7.4 phosphate buffer solution, and 0.1 mol L^{-1} KCl (Figure 9). Thus, the Au-rGO-based 3D printed platform has been used to provide optimal parameters for BPA determination from biological samples collected from children.

Effect of pH on the oxidation of BPA

The effect of pH on the oxidation response of 1×10^{-3} mol L^{-1} BPA at the surface of developed Au-rGO-based 3D printed platform was investigated using differential pulse

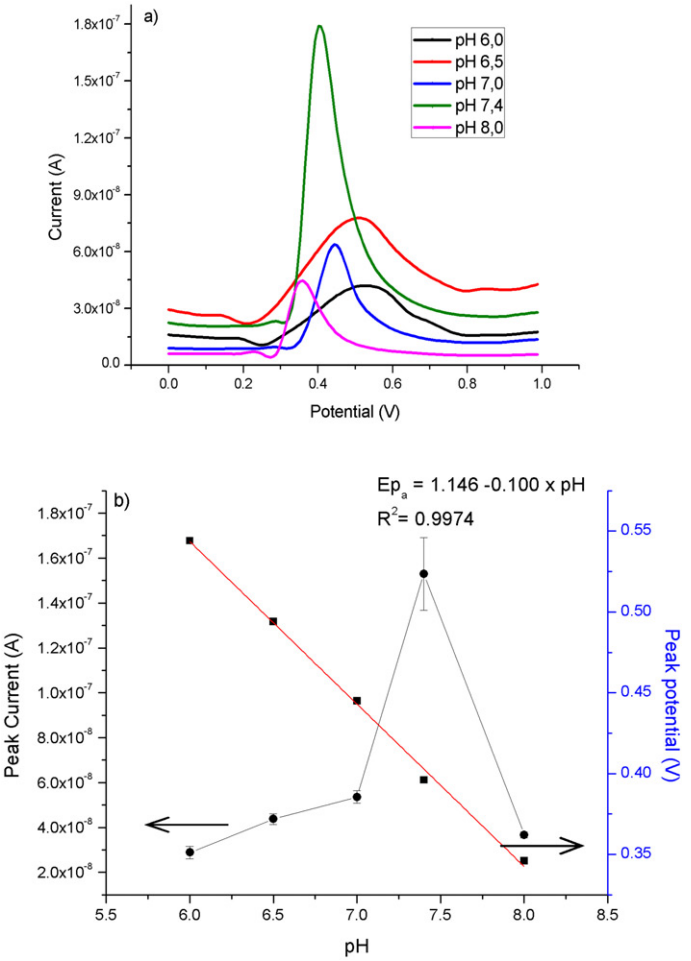

Figure 10. (a) Differential pulse voltammograms of 1×10^{-3} mol L^{-1} BPA at the Au-rGO 3D-printed platform in phosphate buffer solution at pH values of 6.0; 6.5; 7.0; 7.4; and 8.0. (b) Variation of peak current with pH (left) and linear regression of the peak potential with pH (right). Working conditions: step potential of 0.05 V; modulation amplitude of 0.025 V; and a 0.100 V/s scan rate.

voltammetry (Figure 10a). The buffer solutions were prepared as discussed previously at pH values of 6.0; 6.5; 7.0; 7.4; and 8.0. The oxidation potential negatively shifted while the pH value was modified with a maximum peak current at pH 7.4 (Figure 10b, left axis), and was lower than the acid dissociation constant of BPA (pK_{a1}=9.59). BPA is considered to be a weak organic acid, which may dissociate in solution to anionic and dianionic species (Staples et al. 1998), but when the pH is less than the pK_a, the non-dissociated species are predominant in solution (Tian, Wang, and Song 2009). The non-dissociated form of BPA is easily adsorbed to the electrode surface.

The oxidation potential was plotted versus pH (Figure 10b, right axis), providing a linear relationship, described by: E_{pa} (V)=1.146–0.100 pH (R^2 equal to 0.9974), indicating that protons were directly involved in the oxidation of BPA. A pH value of 7.4 is widely used for the electrochemical analysis of different compounds in biological samples and hence was employed for subsequent analytical measurements.

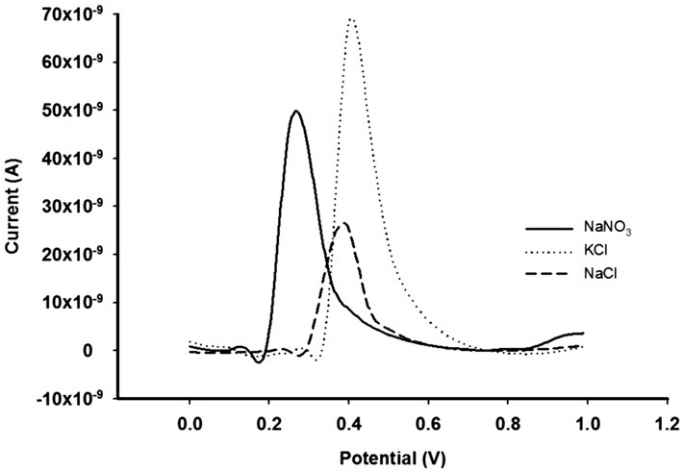

Figure 11. Differential pulse voltammograms in pH 7.4 phosphate buffer solution containing 1.0×10^{-3} mol L^{-1} BPA with three supporting electrolytes: 0.1 mol L^{-1} $NaNO_3$; 0.1 mol L^{-1} KCl; and 0.1 mol L^{-1} NaCl. Working conditions: step potential of 0.05 V; modulation amplitude of 0.025 V; and a 0.100 V/s scan rate.

Effect of supporting electrolyte in determination of BPA using Au-rGO 3D-printed platform

To evaluate the effect of supporting electrolyte in the determination of BPA, differential pulse voltammetry measurements were done in a solution of 1×10^{-3} mol L^{-1} BPA containing phosphate buffer at pH 7.4 and three types of alkaline salts as supporting electrolyte: 0.1 mol L^{-1} $NaNO_3$; 0.1 mol L^{-1} KCl; and 0.1 mol L^{-1} NaCl. Figure 11 shows that an increase in anodic peak current was obtained when 0.1 mol L^{-1} KCl was used, and consequently this material was employed as the supporting electrolyte for further electrochemical measurements of BPA.

Electrochemical response characteristics of Au-rGO composite based 3D-printed platform

Differential pulse voltammetry was used to evaluate the response characteristics of the Au-rGO based 3D printed platform for the BPA oxidation process. Solutions were investigated containing succesive dilutions of BPA from 1×10^{-12} to 1×10^{-2} mol L^{-1} prepared in phosphate buffer at pH 7.4 and 0.1 mol L^{-1} KCl. As it can be seen in Figure 12a, a shift in potential occurred. The shift of BPA peak potential may be caused by a well-known Fouling effect caused by the phenol group due to the adsorption of the oxidation products on the electrode surface (Li et al. 2011).

The increase in the peak current recorded is also directly proportional to the concentration of BPA. The linear calibration plots for both 3D-printed platforms are presented in Figure 12c and show that the peak current recorded for the rGO based 3D printed platform is lower than the peak current recorded for the Au-rGO based 3D printed platform. Also, the Au-rGO based 3D printed platform provided a lower detection limit, 3.52×10^{-9} mol L^{-1}, than 3.05×10^{-6} mol L^{-1} for the rGO based 3D printed platform.

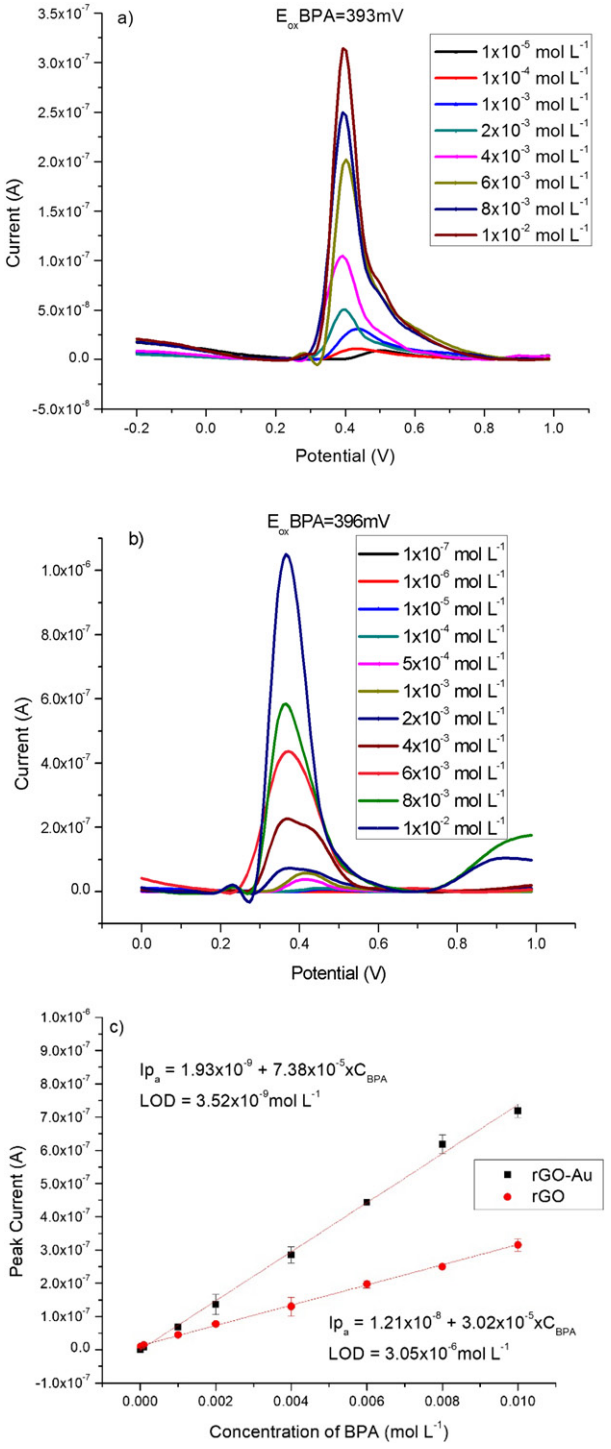

Figure 12. (a) Differential pulse voltammograms with the rGO composite based 3D-platform in BPA solutions from 1×10^{-5} to 1×10^{-2} mol L^{-1}. (b) Differential pulse voltammograms recorded using the Au-rGO composite based 3D-platform in BPA solutions from 1×10^{-5} to 1×10^{-2} mol L^{-1}. (c) Calibration curves obtained using the rGO and Au-rGO composite based 3D-platforms. Working conditions: step potential of 0.05 V; modulation amplitude of 0.025 V; and a 0.100 V/s scan rate.

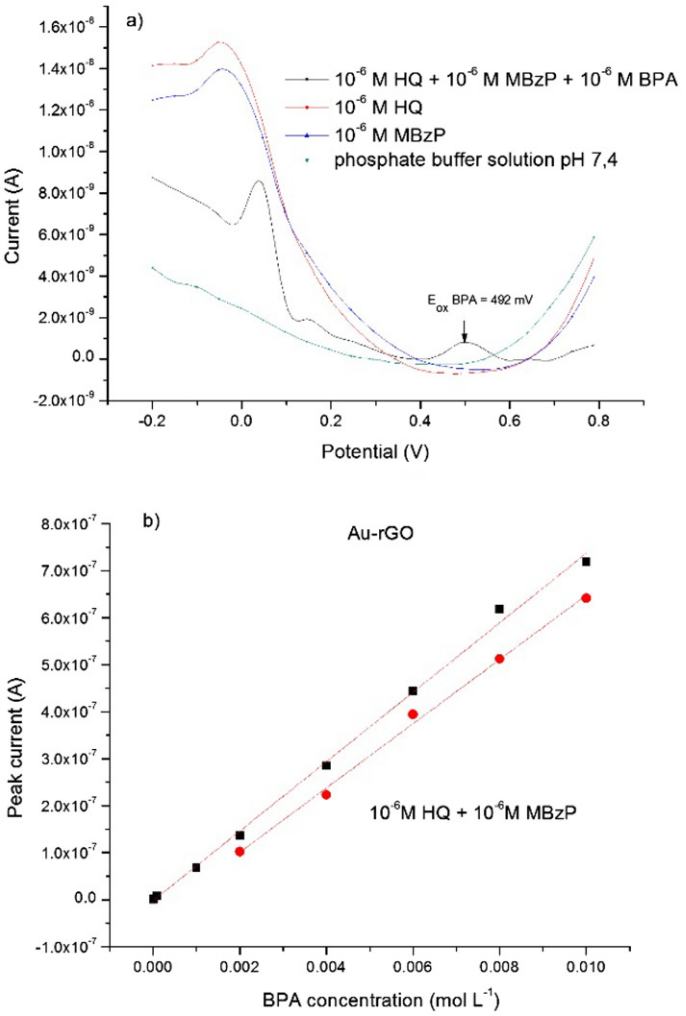

Figure 13. (a) Differential pulse voltammograms obtained with the Au-rGO composite based 3D-platform in pH 7.4 phosphate buffer containing 10^{-6} mol L^{-1} hydroquinone (HQ – red line); 10^{-6} mol L^{-1} monobenzylphthalate (MBzP – blue line); and 10^{-6} mol L^{-1} hydroquinone + 10^{-6} mol L^{-1} monobenzylphthalate + 10^{-6} mol L^{-1} BPA (black line). (b) Calibration relationships showing the linear variation of BPA concentration in the absence (black line) and presence of interfering species: 10^{-6} mol L^{-1} hydroquinone + 10^{-6} mol L^{-1} monobenzylphthalate. Working conditions: step potential of 0.05 V; modulation amplitude of 0.025 V; and a 0.100 V/s scan rate.

Interference study

Hydroquinone (HQ) and monobenzylphthalate (MBzP) were investigated as interfering species to characterize the selectivity of Au-rGO composite based 3D-printed platform for the oxidation of BPA. For this purpose, solutions of the same concentration (1.0×10^{-6} mol L^{-1}) of hydroquinone and monobenzylphthalate were prepared in pH 7.4 phosphate buffer solution and 0.1 mol L^{-1} KCl.

Figure 13a shows the differential pulse voltammograms for pH 7.4 phosphate buffer solution (green line): 1.0×10^{-6} mol L^{-1} hydroquinone (red line); 1.0×10^{-6} mol L^{-1}

Table 5. Determination of BPA in saliva samples from children in correlation with body mass index, age and gender.

Sample	Body mass index percentile	Age (years)	Gender	Measured BPA (μmol L^{-1})
1	88th	12	F	17.0 ± 2.3
2	43rd	14	F	6.48 ± 0.8
3	>95th	11	F	40.2 ± 9.3
4	>95th	10	M	33.1 ± 0.3
5	>95th	11	M	19.7 ± 7.9

monobenzylphthalate (blue line); and 1.0×10^{-6} mol L^{-1} hydroquinone + 1.0×10^{-6} mol L^{-1} monobenzylphthalate + 1.0×10^{-6} mol L^{-1} BPA (black line). In the mixed solution, a single oxidation peak appears for both interfering species (E of 0.05 V) shifted towards more positive potential, while the oxidation for each species alone occurs at E equal to –0.05 V. Also, in the mixed solution, the oxidation of BPA may be observed at the same potential E of 492 mV as in a solution of BPA without interfering species. In Figure 11, for 1.0×10^{-6} mol L^{-1}, the BPA oxidation occurs at E equal to 496 mV.

Figure 13b shows that the addition of interfering species, hydroquinone and monobenzylphthalate, reduces the peak current of the BPA oxidation, even when the lower concentration is not distinguishable.

Analytical applications

The main application of the developed 3D printed platform based on Au-rGO was to evaluate the levels of BPA in pre-pubertal children saliva samples to predict precocious installation of puberty because BPA is an endocrine disrupting chemical. For this purpose, five saliva samples collected from pre-pubertal, bottle fed, obese or over-weight children were investigated, knowing the correlation of childhood obesity and precocious puberty. In this study, high body mass index values were correlated with high levels of BPA in saliva samples (Table 5).

Childhood obesity is one of the main factors for reaching puberty at early ages and coupled with BPA exposure. Obese children are most likely to develop secondary sexual characteristics earlier than normal weight children (Burt Solorzano and McCartney, 2010). BPA is found in many products with which children come in contact and affects the hypothalamic–pituitary axis, by sending false signals to produce gonadotropins, which are responsible for the maturation of sexual organs.

Conclusion

A novel gold-reduced graphene oxide nanocomposite was used for the fabrication of a 3D-printed platform employed in the determination of BPA from saliva samples collected from children. The gold nanoparticles exhibit an enhancement BPA oxidation and provide a low detection limit and high sensitivity. For this reason, the proposed method was successfully applied in the analysis of saliva samples collected from children to evaluate the predisposition to reach puberty at early ages.

Funding

This work was supported by the Ministry of Research and Innovation, CNCS-UEFISCDI, under Grant Number PN-III-P1-1.1-PD-2016-0190, within PNCDI III.

References

Adams, R. N. 1958. Carbon Paste Electrodes. *Analytical Chemistry* 30(9):1576–. doi:10.1021/ac60141a600

Bard, A. J., and L. R. Faulkner. 1980. *Electrochemical methods: fundamentals and applications*, 324–53. New York: Wiley

Berger, K., B. Eskenazi, K. Kogut, K. Parra, R. H. Lustig, L. C. Greenspan, N. Holland, A. M. Calafat, K. Ye, and K. G. Harley. 2018. Association of prenatal urinary concentrations of phthalates and bisphenol A and pubertal timing in boys and girls. *Environmental Health Perspectives* 126:97004.

Bharath, G., R. Madhu, S. M. Chen, V. Veeramani, D. Mangalaraj, and N. Ponpandian. 2015. Solvent-free mechano-chemical synthesis of graphene oxide and Fe_3O_4–reduced graphene oxide nanocomposites for sensitive detection of nitrite. *Journal of Materials Chemistry A* 3(30): 15529–39. doi:10.1039/C5TA03179F.

Bhuyan, S. A., N. Uddin, M. Islam, F. A. Bipasha, and S. S. Hossain. 2016. Synthesis of graphene. *International Nano Letters* 6(2):65–83. doi:10.1007/s40089-015-0176-1.

Burt Solorzano, C. M., and C. R. McCartney. 2010. Obesity and the pubertal transition in girls and boys. *Reproduction* (Cambridge, England) 140(3):399–410. doi:10.1530/REP-10-0119.

Canevari, T. C., M. V. Rossi, and A. D. P. Alexiou. 2019. Development of an electrochemical sensor of endocrine disruptor bisphenol A by reduced graphene oxide for incorporation of spherical carbon nanoparticles. *Journal of Electroanalytical Chemistry* 832:24–30. doi:10.1016/j.jelechem.2018.10.044.

Centers for Disease Control and Prevention. 2019. January 3, https://www.cdc.gov/healthyweight/bmi/calculator.html

DiVall, S. A. 2013. The influence of endocrine disruptors on growth and development of children. *Current Opinion in Endocrinology Diabetes and Obesity* 20(1):50–5. doi:10.1097/MED.0b013e32835b7ee6.

Fan, H., Y. Li, D. Wu, H. Ma, K. Mao, D. Fan, B. Du, H. Li, and Q. Wei. 2012. Electrochemical bisphenol A sensor based on N-doped graphene sheets. *Analytica Chimica Acta* 711:24–8. doi:10.1016/j.aca.2011.10.051.

Frutiger, A., J. T. Muth, D. M. Vogt, Y. Menguc, A. Campo, A. D. Valentine, C. J. Walsh, and J. A. Lewis. 2015. Capacitive soft strain sensors via multicore-shell fiber printing. *Advanced Materials* 27(15):2440–6. doi:10.1002/adma.201500072.

Ganesh, V., S. Pitchumani, and V. Lakshminarayanan. 2006. New symmetric and asymmetric supercapacitors based on high surface area porous nickel and activated carbon. *Journal of Power Sources* 158(2):1523–32. doi:10.1016/j.jpowsour.2005.10.090.

Goldman, L., H. Falk, P. J. Landrigan, S. J. Balk, J. R. Reigart, and R. A. Etzel. 2004. Environmental paediatrics and its impact on government health policy. *Pediatrics* 113(4 Suppl):1146–57.

Huang, N. M. Liu, H. Li, Y. Zhang, and S. Yao. 2015. Synergetic signal amplification based on electrochemical reduced graphene oxide-ferrocene derivative hybrid and gold nanoparticles as an ultra-sensitive detection platform for bisphenol A. *Analytica Chimica Acta* 853 :249–57. doi:10.1016/j.aca.2014.10.016

Huang, W. 2005. Voltammetric determination ofbisphenol A using a carbon paste electrode based on the enhancement effect ofcetyltrimethylammonium bromide (CTAB). *Bulletin of the Korean Chemical Society* 26 :1560–4.

Huang, W. 2005. Voltammetric determination ofbisphenol A using a carbon paste electrode based on the enhancement effect ofcetyltrimethylammonium bromide (CTAB). *Bulletin of the Korean Chemical Society* 26 :1560–4.

Ianesko, F., C. Alves de Lima, C. Antoniazzi, E. R. Santana, J. V. Piovesan, A. Spinelli, A. Galli, and E. Guimaraes de Castro. 2018. Simultaneous electrochemical determination of hydroquinone and bisphenol A using a carbon paste electrode modified with silver nanoparticles. *Electroanalysis* 30(9):1946–55. doi:10.1002/elan.201800074.

Igrec, B., M. Bosiljevac, Z. Sipus, D. Babic, and S. Rudan. 2016. Fiber optic vibration sensor for high-power electric machines realized using 3D printing technology. In *Proceedings of the SPIE 9754*. http://proceedings.spiedigitallibrary.org/

Inoue, K., K. Kato, Y. Yoshimura, T. Makino, and H. Nakazawa. 2000. Determination of bisphenol A in human serum by high-performance liquid chromatography with multi-electrode electrochemical detection. *Journal of Chromatography B* 749(1):17–23. doi:10.1016/S0378-4347(00)00351-0.

Jerance, N., N. Bednar, and G. Stojanovic. 2013. An ink-jet printed eddy current position sensor. *Sensors* (Basel, Switzerland) 13(4):5205–19. doi:10.3390/s130405205.

Jun, S. C. 2015. Fundamental of graphene. In *Graphene-based energy devices*. ed A. Rashid Bin Mohd Yusof, 1–48. 1st ed. Weinheim, Germany: Wiley-VCH Verlag GmbH&Co.

Kadimisetty, K.,. I. M. Mosa, S. Malla, J. E. Satterwhite-Warden, T. M. Kuhns, R. C. Faria, N. H. Lee, and J. F. Rusling. 2016. 3D-printed supercapacitor-powered electrochemiluminescent protein immunoarray. *Biosensors and Bioelectronics* 77:188–93. doi:10.1016/j.bios.2015.09.017.

Kalambate, P. K., C. R. Rawool, S. P. Karna, and A. K. Srivastava. 2016. Highly sensitive and selective determination of methylergometrine maleate using carbon nanofibers/silver nanoparticles composite modified carbon paste electrode. *Material Science and Engineering C* 69: 453–61. doi:10.1016/j.msec.2016.06.077.

Kesner, S. B, and R. D. Howe. 2011. Design Principles for Rapid Prototyping Forces Sensors using 3D Printing. *IEEE/ASME Transactions on Mechatronics : a Joint Publication of the IEEE Industrial Electronics Society and the ASME Dynamic Systems and Control Division* PP(99):1–5. 21874102 doi:10.1109/TMECH.2011.2160353

Kit-Anan, W., A. Olarnwanich, C. Sriprachuabwong, C. Karuwan, A. Tuantranont, A. Wisitsoraat, W. Srituravanich, and A. Pimpin. 2012. Disposable paper-based electrochemical sensor utilizing inkjet-printed polyanilin modified screen-printed carbon electrode for ascorbic detection. *Journal of Electroanalytical Chemistry* 685:72–8. doi:10.1016/j.jelechem.2012.08.039.

Kuklenyik, Z., J. Ekong, C. D. Cutchins, L. L. Needham, and A. M. Calafat. 2003. Simultaneous measurement of urinary bisphenol A and alkylphenols by automated solid-phase extractive derivatization gas chromatography/mass spectrometry. *Analytical Chemistry* 75(24):6820–5. doi:10.1021/ac0303158.

Laszczak, P., L. Jiang, D. L. Bader, D. Moser, and S. Zahedi. 2015. Development and validation of a 3D-printed interfacial stress sensor for prosthetic applications. *Medical Engineering and Physics* 37:32–137.

Lei, Y., L. Fang, M. S. H. Akash, Z. Liu, W. Shi, and S. Chen. 2013. Development and comparison of two competitive ELISAs for the detection of bisphenol A in human urine. *Analytical Methods* 5(21):6106–13. doi:10.1039/c3ay41023d.

Leonardi, A., M. Cofini, D. Rigante, L. Lucchetti, C. Cipolla, L. Penta, and S. Esposito. 2017. The effect of bisphenol A on puberty: A critical review of the medical literature. *International Journal of Environmental Research and Public Health* 14(9):1044. doi:10.3390/ijerph14091044.

Li, J., D. Kuang, Y. Feng, F. Zhang, and M. Liu. 2011. Voltammetric determination of bisphenol A in food package by a glassy carbon electrode modified with carboxylated multi-walled carbon nanotubes. *Microchimica Acta* 172(3–4):379–86. doi:10.1007/s00604-010-0512-0.

Li, Y., X. Zhai, X. Liu, L. Wang, H. Liu, and H. Wang. 2016. Electrochemical determination of bisphenol A ar ordered mesoporous carbon modified nano-carbon ionic liquid paste electrode. *Talanta* 148:362–9. doi:10.1016/j.talanta.2015.11.010.

Lind, J. U., T. A. Busbee, A. D. Valentine, F. S. Pasqualini, H. Yuan, M. Yadid, S.-J. Park, A. Kotikian, A. P. Nesmith, P. H. Campbell., et al. 2017. Instrumented cardiac microphysiological

devices via multimaterial three-dimensional printing. *Nature Materials* 16(3):303–8. doi:10.1038/nmat4782.

Mandoon, C. A., L. J. Blum, and C. A. Marquette. 2016. Adding biomolecular recognition capability to 3D-printed objects. *Analytical Chemistry* 88:10767–72. doi:10.1021/acs.analchem.6b03426.

Messaoud, B. N., M. E. Ghica, C. Dridi, M. B. Ali, and C. M. A. Brett. 2017. Electrochemical sensor baed on Multiwalled carbon nanotubes and gold nanoparticles modified electrode for the sensitive detection of bisphenol A. *Sensors and Actuators B* 253:513–22. doi:10.1016/j.snb.2017.06.160.

Morgan, M. K., P. A. Jones, A. M. Calafat, X. Ye, C. W. Croghan, J. C. Chuang, N. K. Wilson, M. S. Clifton, Z. Figueroa, and L. S. Sheldon. 2011. Assessing the quantitative relationships between preschool children's exposure to bisphenol A by route and urinary biomonitoring. *Environmental Science and Technology* 45(12):5309–16. doi:10.1021/es200537u.

Nkosi, D., J. Pillay, K. I. Ozoemena, K. Nouneh, and M. Oyama. 2010. Heterogeneous electron transfer kinetics and electrocatalytic behaviour of mixed self-assembled ferrocenes and SWCNT layers. *Physical Chemistry Chemical Physics* 12(3):604–13. doi:10.1039/b918754e.

Ouchi, K., and S. Watanabe. 2002. Measurement of bisphenol A in human urine using liquid chromatography with multi-channel coulometric electrochemical detection. *Journal of Chromatography B* 780(2):365–70. doi:10.1016/S1570-0232(02)00547-0.

Parnianchi, F., M. Nazari, J. Maleki, and M. Mohebi. 2018. Combination of graphene and graphene oxide with metal and metal oxide nanoparticles in fabrication of electrochemical enzymatic biosensors. *International Nano Letters* 8(4):229–39. doi:10.1007/s40089-018-0253-3.

Pogacean, F., A. R. Biris, C. Socaci, M. Coros, L. Magerusan, M. C. Rosu, M. D. Lazar, G. Borodi, and S. Pruneanu. 2016. Graphene–bimetallic nanoparticle composites with enhanced electro-catalytic detection of bisphenol A. *Nanotechnology* 27(48):484001. doi:10.1088/0957-4484/27/48/484001.

Portaccio, M., A. Di Tuoro, F. Arduini, M. Lepore, D. G. Mita, N. Diano, L. Mita, and D. Moscone. 2010. A thionine-modified carbon paste amperometric biosensor for cathecol and bisphenol A determination. *Biosensors and Bioelectronics* 25(9):2003–8. doi:10.1016/j.bios.2010.01.025.

Pruneanu, S., A. R. Biris, F. Pogacean, C. Socaci, M. Coros, M. C. Rosu, F. Watanabe, and A. S. Biris. 2015. The influence of uric and ascorbic acid on the electrochemical detection of dopamine using graphene-modified electrodes. *Electrochimica Acta* 154:197–204. doi:10.1016/j.electacta.2014.12.046.

Sajiki, J., K. Takahashi, and J. Yonekubo. 1999. Sensitive method for the determination of bisphenol A in serum using two systems of high-performance liquid chromatography. *Journal of Chromatography B* 736(1–2):255–61. doi:10.1016/S0378-4347(99)00471-5.

Sanz-Izquierdo, B., and E. A. Parker. 2014. 3-D printing of elements in frequency selective arrays. *IEEE Transactions on Antennas and Propagation* 62(12):6060–6. doi:10.1109/TAP.2014.2359470.

Shi, R., J. Liang, Z. Zhao, A. Liu, and Y. Tian. 2017. An electrochemical bisphenol A sensor based on one step electrochemical reduction of cuprous wrapped graphene oxide nanoparticles modified electrode. *Talanta* 169:37–43. doi:10.1016/j.talanta.2017.03.042.

Sidwaba, U., N. Ntshongontshi, U. Feleni, L. Wilson, T. Waryo, and E. I. Iwuoha. 2019. Manganese peroxidase-based electro-oxidation on bisphenol A at hydrogellic polyaniline–titania nanocomposite-modified glassy carbon electrode. *Electrocatalysis.* https://doi.org/10.1007/s12678-019-0510-x

Srinivas, G., Y. Zhu, R. Piner, N. Skipper, M. Ellerby, and R. Ruoff. 2010. Synthesis of graphene-like nanosheets and their hydrogen adsorption capacity. *Carbon* 48(3):630–5. doi:10.1016/j.carbon.2009.10.003.

Staples, C. A., P. B. Dorn, G. M. Klecka, S. T. O'Block, and L. R. Harris. 1998. A review of the environmental fate, effects, and exposure of bisphenol A. *Chemosphere* 36(10):2149–73.

Staymates, M. E., W. A. MacCrehan, J. L. Staymates, R. R. Kunz, T. Mendum, T. H. Ong, G. Geurtsen, G. J. Gillen, and B. A. Craven. 2016. Biomimetic sniffing improves the detection

performance of a 3D-printed nose of a dog and a commercial trace vapour detector. *Scientific Reports* 6:36876.

Stefan-van Staden, R.-I., L. A. Gugoaşă, B. Calenic, J. F. van Staden, and J. Legler. 2014. Screening of children saliva samples for bisphenol A using stochastic, amperometric and multimode microsensors. *Analytical Chemistry Research* 1:1–7. doi:10.1016/j.ancr.2014.06.001.

Sun, Y., M. Irie, N. Kishikawa, M. Wada, N. Kuroda, and K. Nakashima. 2004. Determination of bisphenol A in human breast milk by HPLC with column-switching and fluorescence detection. *Biomedical Chromatography* 18(8):501–7. doi:10.1002/bmc.345.

Tian, C., J. T. Wang, and X. L. Song. 2009. Sediment–water interactions of bisphenol A under simulated marine conditions. *Water, Air, and Soil Pollution* 199(1-4):301–10. doi:10.1007/s11270-008-9879-5.

Tsukioka, T.,. J. Brock, S. Graiser, J. Nguyen, H. Nakazawa, and T. Makino. 2003. Determination of trace amounts of bisphenol A in urine by negative-ion-chemical-ionization-gas chromatography/mass spectrometry. *Analytical Sciences* 191:151–3. doi:10.2116/analsci.19.151.

Vandenberg, L. N., I. Chahoud, J. J. Heindel, V. Padmanabhan, F. J. R. Paumgartten, and G. Schoenfelder. 2010. Urinary, circulating and tissue biomonitoring studies indicate widespread exposure to bisphenol A. *Environmental Health Perspectives* 118(8):1055–70. doi:10.1289/ehp.0901716.

Wan, J., Y. X. Si, C. Li, and C. Zhang. 2016. Bisphenol A electrochemical sensors based on multi-walled carbon nanotubes/polythiophene/Pt nanocomposites modified electrode. *Analytical Methods* 8(16):3333–8. doi:10.1039/C6AY00850J.

Wang, Y. C., D. Cokeliler, and S. Gunasekaran. 2015. Reduced graphene oxide/carbon nanotube/gold nanoparticles nanocomposite functionalized screen-printed electrode for sensitive electrochemical detection of endocrine disruptor bisphenol A. *Electroanalysis* 27(11):2527–36. doi:10.1002/elan.201500120.

Watanabe, T., H. Yamamoto, K. Inoue, A. Yamaguchi, Y. Yoshimura, K. Kato, H. Nakazawa, N. Kuroda, and K. Nakashima. 2001. Development of sensitive high-performance liquid chromatography with fluorescence detection using 4-(4,5-diphenyl-1H-imidazol-2-yl)-benzoul chloride as a labelling reagent for determination of bisphenol A in plasma samples. *Journal of Chromatography B* 762(1):1–7. doi:10.1016/S0378-4347(01)00287-0.

Watkins, D. J., B. N. Sanchez, M. M. Tellez-Rojo, J. M. Lee, A. Mercado-Garcia, C. Blank-Goldenberg, K. E. Peterson, and J. D. Meeker. 2017. Phthalate and bisphenol A exposure during *in utero* windows of susceptibility in relation to reproductive hormones and pubertal development in girls. *Environmental Research* 159:143–51. doi:10.1016/j.envres.2017.07.051.

Xu, J., Y. Wang, and S. Hu. 2017. Nanocomposites of graphene and graphene oxides: Synthesis, molecular functionalization and application in electrochemical sensors and biosensors. A review. *Microchimica Acta* 184(1):1–44. doi:10.1007/s00604-016-2007-0.

Xu, Y., X. Wu, X. Guo, B. Kong, M. Zhang, X. Qian, S. Mi, and W. Sun. 2017. The boom in 3D-printed sensor technology. *Sensors* 17(5):1166. doi:10.3390/s17051166.

Yamada, H., I. Furuta, E. H. Kato, S. Kataoka, Y. Usuki, G. Kobashi, F. Sata, R. Kishi, and S. Fujimoto. 2002. Maternal serum and amniotic fluid bisphenol A concentrations in the early second trimester. *Reproductive Toxicology* 16(6):735–9. doi:10.1016/S0890-6238(02)00051-5.

Yang, L., H. Zhao, S. M. Fan, B. C. Li, and P. C. Li. 2014. A highly sensitive electrochemical sensor for simultaneous determination of hydroquinone and bisphenol A based on the ultrafine Pd nanoparticle @ TiO_2 functionalized SiC. *Analytica Chimica Acta* 852 :28–36. doi:10.1016/j.aca.2014.08.037.

Yang, S. H., A. A. Morgan, H. P. Nguyen, H. Moore, B. J. Figard, and K. A. Schug. 2011. Quantitative determination of bisphenol A from human saliva using bulk derivatization and trap-and-elute liquid chromatography coupled to electrospray ionization mass spectrometry. *Environmental Toxicology and Chemistry* 30(6):1243–51. doi:10.1002/etc.498.

Yin, H. S., Y. L. Zhou, and S. Y. Ai. 2009. Preparation and characterization of cobalt phtalocyanince modified carbon paste electrode for bisphenol A detection. *Journal of Electroanalytical Chemistry* 626(1–2):80–8. doi:10.1016/j.jelechem.2008.11.004.

Yu, X. W., Y. K. Chen, L. P. Chang, L. Zhou, F. X. Tang, and X. P. Wu. 2013. β-cyclodextrin non-covalently modified ionic liquid-based carbon paste electrode as a novel voltammetric sensor for specific detection of bisphenol A. *Sensors and Actuators B* 186:648–56. doi:10.1016/j.snb.2013.06.089.

Yu, Z., Y. Luan, H. Li, W. Wang, X. Wang, and Q. Zhang. 2019. A disposable electrochemical aptasensor using single-stranded DNA-methylene blue complex as signal-amplification platform for sensitive sensing of bisphenol A. *Sensors and Actuators B* 284:73–80. doi:10.1016/j.snb.2018.12.126.

Zanello, P. 2003. Inorganic Electrochemistry:Theory, Practice and Application. *Cambridge: The Royal Society of Chemistry*

Zhu, L. L., Y. H. Cao, and G. Q. Cao. 2014. Electrochemical sensor based on magnetic molecularly imprinted nanoparticles at surfactant modified magnetic electrode for determination of bisphenol A. *Biosensors and Bioelectronics* 54:258–61.

Zhu, Y., C. Zhou, X. Yan, Y. Yan, and Q. Wang. 2015. Aptamer-functionalized nanoporous gold film for high-performance direct electrochemical detection of bisphenol A in human serum. *Analytica Chimica Acta* 883:81–9. doi:10.1016/j.aca.2015.05.002.